Journal of Rock Mechanics and Geotechnical Engineering 13 (2021) 311–320

Contents lists available at ScienceDirect

Journal of Rock Mechanics and Geotechnical Engineering

journal homepage: www.jrmge.cn

Full Length Article

Assessment of the properties of polycrystalline rock salt synthesized under nominally dry and wet conditions

Amirsalar Moslehy*, Khalid Alshibli

Department of Civil and Environmental Engineering, University of Tennessee, Knoxville, TN, 37996, USA

ARTICLE INFO

Article history:
Received 11 April 2020
Received in revised form
14 August 2020
Accepted 9 September 2020
Available online 2 December 2020

Keywords:
Halite
Rock salt
Unconfined compression
One-dimensional (1D) compression

ABSTRACT

Polycrystalline rock salt's compression is a function of applied stresses, exposure duration to the applied stresses, ambient temperature, and water content. Rock salt's compressional behavior under different conditions and its effects on the specimens' mechanical properties have been investigated in the literature. However, the one-dimensional (1D) compression behavior of polycrystalline rock salt at various water contents and how the specimen's compression at different water contents further affects its physical and mechanical properties are not fully understood yet. In this study, polycrystalline rock salt specimens were prepared under nominally dry and wet conditions and some of the dry and wet specimens were annealed after the preparation. The relationship between the porosity of the specimens and the logarithm of the applied axial stresses during the 1D compression was found to follow a linear relationship after reaching unique critical porosities of 32% and 37% for the dry and wet specimens, respectively. Unloading and reloading the specimens did not result in any major changes in the porosity of the specimens. The specimens compressed under wet condition showed an average final porosity of 2.6% compared to 6.9% for the dry specimens. The dry and wet specimens that were annealed after the compression exhibited a lower porosity in comparison to the dry and wet specimens, respectively. Unconfined compression experiments on the specimens showed dry and wet specimens possess averaged unconfined compressive strengths (σ_u) of 64.3 and 16.2 MPa, respectively. Annealing decreased σ_u of the dry specimens to 39.6 MPa and increased σ_u of the wet specimens to 41 MPa.

1. Introduction

Rock salt, or halite, is a sedimentary rock formed by evaporation of bodies of water (Dusseault et al., 2004). Therefore, rock salt formations are mostly bedded, and can have impurities (Hansen and Leigh, 2011; Titler and Curry, 2011) and develop into salt domes depending on the tectonic pressures and movements because of their lower density compared to their surrounding materials (Trusheim, 1960; Sannemann, 1968; Dronkert and Remmelts, 1996). Rock salt formations, bedded or dome-shaped, usually have low permeability and porosity; therefore, they are mainly used as repositories for hazardous waste or oil storage (Urai et al., 1986; Pouya, 1991; Fam et al., 1998; Hunsche and Hampel, 1999; Marques et al., 2013). The conditions imposed on rock salt deposits during their compressions such as temperature, time, pressure, and presence of humidity or water can influence the density, porosity, and size of the grains of the deposit (Holcomb and Zeuch, 1988; Hwang et al., 1993). Different deformation mechanisms such as dislocation, crystal plasticity, pressure solution, and dynamic recrystallization can be mobilized during the compression. The applied stress during the compression has the most significant effects on rock salt's mechanical properties after the compression. The presence of water during the compression of rock salt can significantly facilitate dislocation, sliding, and pressure solution of salt grains. Conversely, in the absence of humidity, salt grains tend to crush and deform plastically (Hwang et al., 1993; Ding et al., 2016). However, recrystallization of salt grains, especially dynamic recrystallization, does not normally occur at temperatures below 150 °C (Ding et al., 2016; Mills et al., 2018).

Holcomb and Zeuch (1988) investigated the compression of dry crushed rock salt. They used quasi-static compactions and creep tests to evaluate the time-dependent compression of rock salt. The tests were conducted at various temperatures, stresses, and time

* Corresponding author.
E-mail address: amoslehy@vols.utk.edu (A. Moslehy).
Peer review under responsibility of Institute of Rock and Soil Mechanics, Chinese Academy of Sciences.

https://doi.org/10.1016/j.jrmge.2020.09.010

durations. By fitting an empirical model to the results obtained from the test, Holcomb and Zeuch (1988) further developed a plastic yield and power-law creep model to the response of the material. Hwang et al. (1993) employed in situ scanning electron microscopy (SEM) during the compression process to understand the activation of different deformation mechanisms on the compression of rock salt. They found the compression of crushed rock salt is governed by grain crushing and shearing at low water contents and it was controlled by sliding of the grains at higher water contents. Ding et al. (2016) examined the mechanical behavior of dry rock salt during the compression where the tests were performed at various temperatures and along different load paths. The findings were that temperature has the most significant influence on the compression of the material, while the grain size and loading path have limited effects. Moreover, by using reflected light micrographs, they identified the dominant deformation mechanism to be crystal plasticity and found the recrystallization of the material began slowly at temperatures above 150 °C. Mills et al. (2018) performed creep compression tests to investigate the active deformation mechanisms during the compression of rock salt. With the aid of different observational methods, they concluded that the presence of water at or above 1% water content within the specimen would cause the pressure solution to effectively enhance the compression and increase the cohesion of grain boundaries. Shen and Arson (2019) concluded that pressure solution, crystal slip plasticity, and grain boundary sliding are the main deformation mechanisms in axial compression of rock salt at temperatures below 350 °C.

The compression of rock salt further affects its mechanical properties by influencing the grains and grain boundaries of the medium. Grain boundaries are crystallographically defective regions between grains within rock salt formations. Compressed rock salt normally retains 0.01%–1.24% water within its grain boundaries in nature (De Las Cuevas and Pueyo, 1995). The properties of grain boundaries, such as water content, can thus influence the mechanical behavior of compressed rock salt by obstructing or facilitating the movements of the grains (Mouritz, 2012). Moreover, activation of deformation mechanisms such as recrystallization (annealing) and crystal plasticity can affect the properties of the grains, including their size and shape, which influences the mechanical behavior and strength of the medium after the compression (Knudsen, 1959; Ostapenko et al., 1993; Peach et al., 2001). Stormont et al. (2017) compressed polycrystalline rock salt specimens under hydrostatic stresses up to 40 MPa and temperatures up to 250 °C. The results of their work showed that specimens compressed at higher stresses have lower final porosities and therefore lower permeabilities. Moreover, they observed specimens with porosities below a critical porosity value (in the range of 0.02–0.05) did not possess a connected pore network, whereas specimens prepared above the critical porosity had a connected pore network. Paneru et al. (2018) investigated the thermal properties of granular salt specimens made by either compression at high axial stresses at ambient temperature or compression at a longer period of time and elevated temperatures. The specimens that were prepared using the short-time compression method had open grain boundaries with cleavage cracking compared to the long-time compressed specimens with similar porosity which had saturated and fused grain boundaries.

Lebensohn et al. (2003) investigated the deformation and texture development in polycrystalline rock salt by compressing and testing different types of specimens using triaxial extension experiments. The specimens were compressed by cold-pressing rock salt grains at 120 °C and an axial stress of 200 MPa. Selected compressed specimens were then annealed at 650 °C for one day. The comparison of the specimens after the compression showed the annealed specimens had double the average grain size of cold-pressed specimens. Moreover, during triaxial experiments, annealed specimens exhibited a lower compressive strength. Ter Heege et al. (2005) studied the dynamic recrystallization of wet compressed polycrystalline rock salt specimens by axial compression tests. The specimens initially contained 0.1% water content and were cold-pressed at 200 MPa; then, they were cured at 150 °C and 100 MPa axial stress for one week. A set of prepared specimens was annealed at a temperature of 515 °C for one day to make them nominally dry. The triaxial compression tests on the specimens showed more dynamic recrystallization occurred within the wet specimens, and they possessed a lower compressive strength. Liang et al. (2012) tested natural low porosity polycrystalline rock salt specimens under monotonic and cyclic unconfined compression conditions. The specimens tested under monotonic loading condition showed elastoplastic behavior and failed in a ductile manner because the main observed deformation mechanism was grain-sliding along the grain boundaries. Bourcier et al. (2013) investigated crystal plasticity and grain boundary sliding in different types of specimens. Salt grains with two different initial sizes were hot-pressed at a temperature of 150 °C and an axial stress of 100 MPa. Selected prepared specimens with initially coarser grains were annealed at a temperature of 750 °C for two days. Uniaxial compression experiments on the specimens revealed that the recrystallized (annealed) specimens exhibited a lower compressive strength, while the specimens with the minimum initial grain size showed the highest compressive strength. Ding et al. (2017) studied microcrack network development in polycrystalline rock salt under cyclic loading. The specimen showed a dominant elastic behavior during the initial load cycle before yielding, whereas it showed a ductile behavior and deformed plastically with work hardening throughout the next cycles of loading. The plastic deformation of the specimen was attributed to grain boundary microcracks which were preferably oriented in the loading direction. In addition to the grain boundary microcracks, the plastic deformation of the grains is the other main mechanism in rock salt's plastic deformation under axial loading (Müller et al., 2018; Shen et al., 2020).

This paper proposes a simple model to define the relationship between the applied axial stress and porosity in one-dimensional (1D) compression of rock salt under wet and dry conditions. Detailed specimen preparation methods presented in this study are economical, easy to execute, and fast; therefore, they can be used to prepare a large number of polycrystalline rock salt specimens for various studies in the future. Moreover, the reproducibility of the specimens is investigated using micro- and macro-scale methods. Two compression procedures, i.e. dry and wet, were employed to assess the effects of water content on the compression of rock salt. The specimens prepared in dry and wet compression are denoted as dry and wet specimens, respectively. Some of the dry and wet compressed specimens were annealed after the compression and they are labeled as dry-annealed and wet-annealed specimens, respectively. SEM scanning was performed on representative specimens of dry, dry-annealed, and wet-annealed types to study and compare the local porosities and average grain size of differently prepared specimens. Lastly, two specimens of each type were tested using the unconfined compression test to determine their compressive strength.

2. Raw material

Rock salt grains used for specimen preparation in the study were collected from Windsor Salt Mine, Ontario, Canada. Natural non-commercial grade rock salt does not contain any additives such as anticaking agents, which can affect the behavior of the material. Mineralogy and purity of the material were examined by powder X-

ray diffraction method; the composition of the material was 99.9% pure halite. Larger blocks of rock salt were cut and ground to a grain size smaller than 0.075 mm to provide the starting grains for the compression of different types of polycrystalline specimens. Moreover, the initial nominal water content of the starting grains was found to be 0.1% based on ASTM D2216-19 (2019).

3. Compression setup

Stainless-steel tubes with an inner diameter of 25.65 mm, a wall thickness of 3.05 mm, and a height of 76.2 mm were used in this study to prepare specimens with a diameter of approximately 25.65 mm and a height of 50.8 mm. A cylindrical stainless-steel die with an inner diameter of 31.76 mm, a wall thickness of 22.22 mm, and a height of 76.2 mm was used to confine the specimen tubes. A stainless-steel disk of 25.4 mm in diameter and 12.7 mm in height was placed at the bottom of the specimen tubes to prevent contact of specimens with other parts of the setup. A 76.2 mm stainless-steel rod with a diameter of 25.7 mm was used to press the salt grains inside the specimen tubes (Fig. 1a and b). Furthermore, the following parts were used to confine specimens during the annealing process:

(1) A 127 mm × 127 mm square steel plate with a thickness of 19.05 mm and eight 1/2 inches (12.7 mm)-13 threaded holes (bottom plate);
(2) Eight 1/2 inches (12.7 mm)-13 threaded steel rods with lengths of 228.6 mm;
(3) A 127 mm × 127 mm square steel plate with a thickness of 19.05 mm and eight 12.45 mm through holes (top plate);
(4) Eight 1/2 inches (12.7 mm)-13 stainless-steel nuts.

Lastly, another stainless-steel rod with a diameter of 25.7 mm and a height of 76.2 mm was used to transfer the axial stresses to

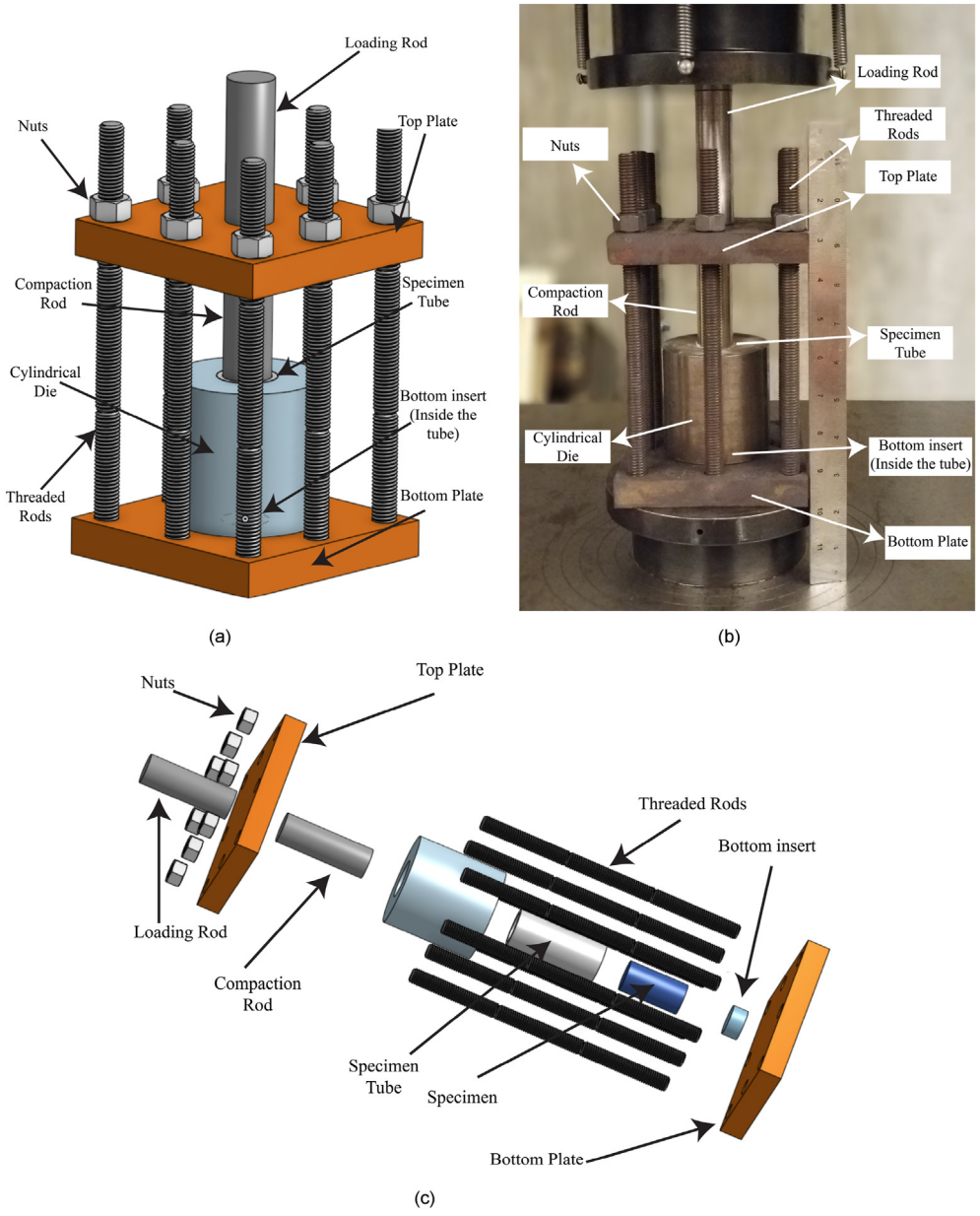

Fig. 1. Specimen compression setup: (a) 3D rendering; (b) Experiment setup; and (c) Exploded view of the parts.

the setup when the compression setup was placed inside the confining system. Fig. 1c shows all the parts used in the compression setup in an exploded view.

4. Specimen compression

Dry specimens (Fig. 2a) were made by cold-pressing the ground salt grains in three layers each with equal thickness. Each layer was compressed using a uniaxial stress of 200 MPa for 20 s. The uniaxial stress was applied at a constant displacement rate of 0.085 mm/s, which is equal to a strain rate of 0.0023 s^{-1}. During the 1D compression of each layer, the specimen was unloaded and then reloaded at 10 MPa and 70 MPa axial stresses to investigate the recoverability of the deformations. The specimen was then compressed at the same uniaxial stress for 1 h after the 1D compression of the final layer. Then, the tube containing the specimen was extruded from the cylindrical die and was cut across its height to split it for easy removal of the specimen. The ends of the specimen were sanded to make them parallel and maintain the cylindrical shape of the specimen. A bedding plane (layer boundary) can be observed on the surface of the specimen between every two consecutive layers (Fig. 2a).

The three layers of dry-annealed specimens, as shown in Fig. 2b, were made similar to the dry specimens, but the confinement parts were used during the 1-h compression of the specimen; thus, the uniaxial stress could be contained on the specimens throughout the annealing process. The setup was then placed in an oven with a temperature of 200 °C for 7 d. The specimens were extruded and sanded using a procedure similar to the dry specimens. Dry-annealed specimens also showed bedding planes between the consecutive layers as well (Fig. 2b).

Wet and wet-annealed specimens were composed of the salt grains and salt-saturated de-aired deionized water with a ratio of 75%–25%, respectively. Deionized water saturated with salt was used to prevent the addition of any substances to the specimens and to prevent the water from dissolving the salt grains within the specimens. Salt grains were added to the de-aired deionized water until the solution could not dissolve more salt grains and the addition of more salt grains would result in the settlement of the added salt grains. The mixture of salt and salt-saturated de-aired deionized water was cold-pressed and annealed (in case of wet-annealed specimens) in the same manner used in the preparation of dry and dry-annealed specimens. The specimen was extruded from the specimen tube and was sanded to maintain its cylindrical shape (Fig. 2c and d). Wet and wet-annealed specimens did not exhibit any bedding planes being formed between the consecutive layers of compression showing more interconnection between the grain boundaries of the consecutive layers. Table 1 summarizes the dimensions, weights, and global porosities of eight specimens, two of each type, measured after compression while being prepared for unconfined compression experiments.

Fig. 3a and b shows the porosity (ϕ) of the specimen versus the applied axial stress (σ_1) during the 1D compression of all layers for two dry and two wet specimens, respectively. B, M, and T in Fig. 3 legend refer to the bottom, middle, and top layers of each specimen, respectively, while F denotes the final compression on the whole specimen. The porosities of the specimens were calculated from the measured axial deformations knowing the volume change of the specimens occurred only due to axial deformations. Moreover, the elastic (recoverable) volume change of the grains during the 1D compression was neglected because of the difficulties of measuring the volume change of the grains in the experimental setup used in this study. Comparing the results obtained from the dry 1D compression of the different layers of a dry specimen (D_1 or D_2), the relationship of ϕ with σ_1 follows a unique decaying exponential curve. The uniqueness of the exponential curve describing ϕ of the specimen versus σ_1 shows during the 1D compression of a layer, the layers compressed previously (which were being reloaded) did not exhibit a significant deformation. Eq. (1) is a decaying exponential fit to the loading curves of ϕ versus σ_1 of the dry specimens with a coefficient of determination (R^2) of 0.997. Moreover, a comparison between the results obtained from the 1D compression of specimens D_1 and D_2 demonstrates no statistical difference between the results obtained from each specimen, which shows the reproducibility of the compression procedure. Referring to Fig. 3b, the results obtained from different layers of the two wet specimens W_1 and W_2 are similar and provide the same findings as to the dry specimens. Eq. (2) describes the relationship of ϕ versus σ_1 for wet specimens.

Table 1
Physical properties of polycrystalline rock salt specimens.

Specimen	Height (mm)	Diameter (mm)	Mass (g)	Porosity (%)
D_1 (dry)	51.8	25.9	55.21	6.8
D_2 (dry)	53.5	25.9	57.14	6.9
DA_1 (dry-annealed)	50	25.4	54.03	1.6
DA_2 (dry-annealed)	50.4	26	57.37	1.5
W_1 (wet)	46.1	25.9	51.24	2.8
W_2 (wet)	43.6	25.9	48.63	2.4
WA_1 (wet-annealed)	40.5	25.5	44.46	0.7
WA_2 (wet-annealed)	48.2	24.6	49.09	1

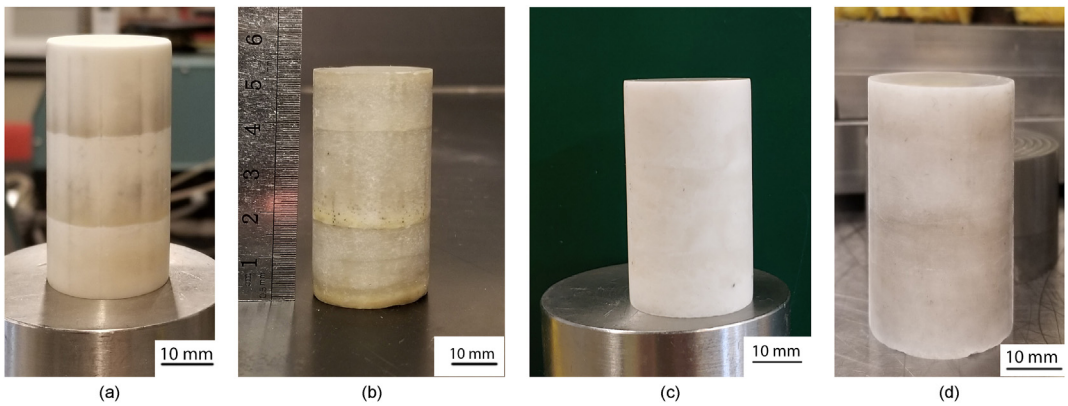

Fig. 2. Polycrystalline rock salt specimens: (a) Dry; (b) Dry-annealed; (c) Wet; and (d) Wet-annealed.

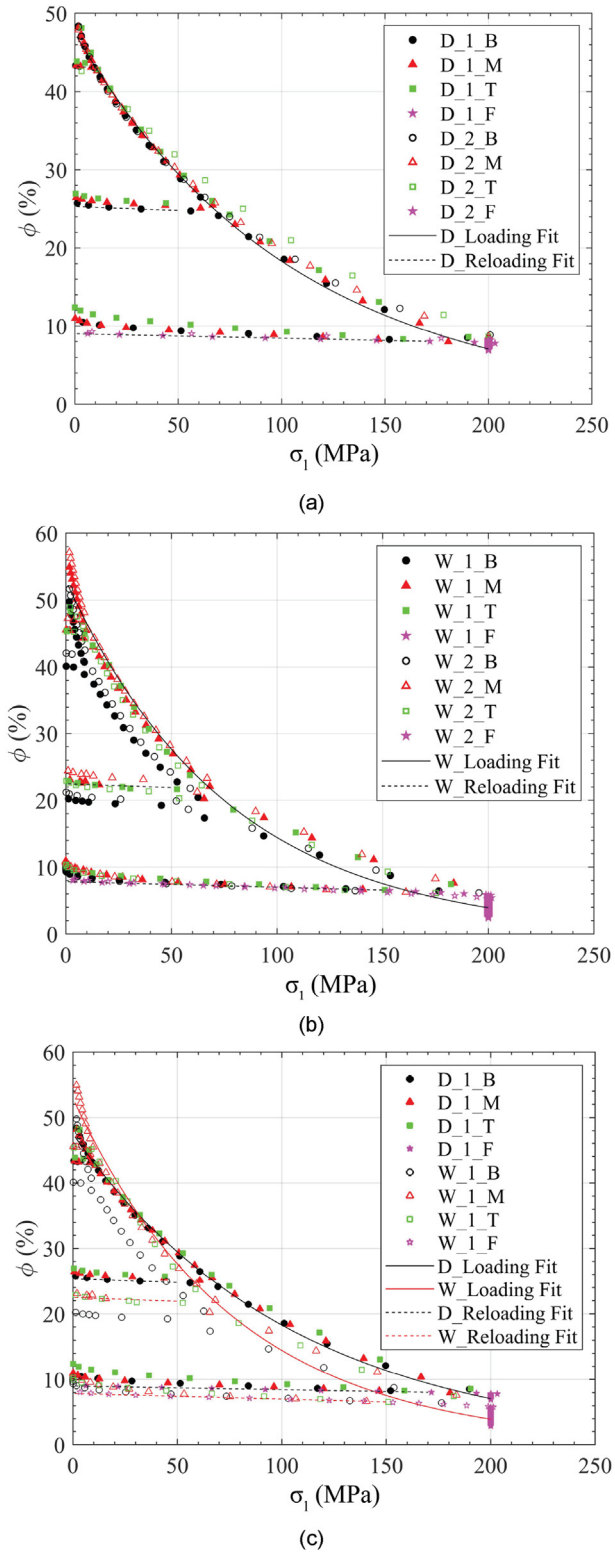

Fig. 3. Porosity versus axial stress during the compression of (a) dry, (b) wet, and (c) dry and wet specimens.

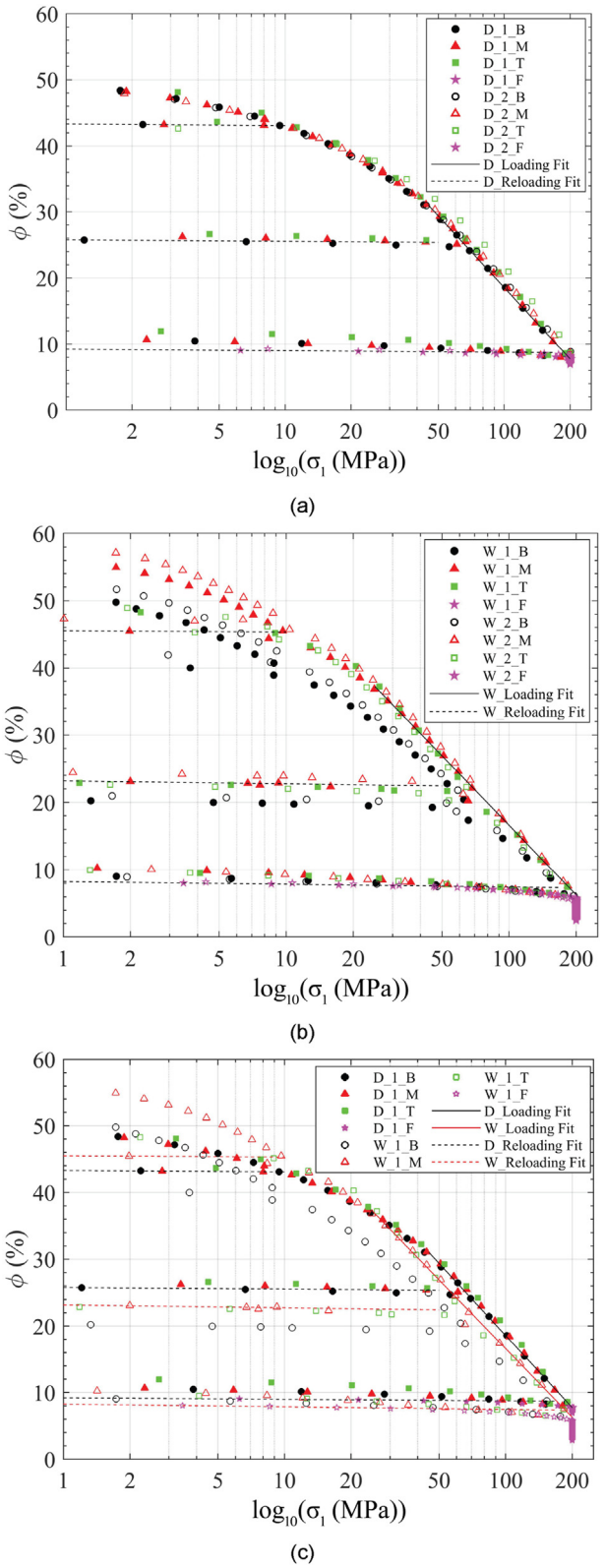

Fig. 4. Porosity versus axial stress' logarithm during the 1D compression of (a) dry, (b) wet, and (c) dry and wet specimens.

$$\phi_L = 47.45 \exp(-0.00956\sigma_1) \quad \left(R^2 = 0.997\right) \tag{1}$$

$$\phi_L = 52.93 \exp(-0.013\sigma_1) \quad \left(R^2 = 0.985\right) \tag{2}$$

The final 1D compression of both types of compression (reloading the whole specimen) or the unloading-reloading curves of the 1D compression display a linear relationship between ϕ and

σ_1. Eqs. (3) and (4) represent the slope of the fitted lines for dry and wet 1D compression unloading and reloading phases of the experiments, respectively. The change in the porosity of the specimens during the unloading-reloading is due to the elastic deformation of the grains which is considered negligible when compared to the non-recoverable deformations.

$$\phi_R = -0.01\sigma_1 \quad \left(R^2 = 0.979\right) \tag{3}$$

$$\phi_R = -0.011\sigma_1 \quad \left(R^2 = 0.958\right) \tag{4}$$

Fig. 3c compares the 1D compression results of dry specimen D_1 and wet specimen W_1 and shows that the wet specimens' porosities decreased at a steeper rate than dry specimens' porosities both during the loading and reloading of the material. Because the applied strain rate during the 1D compression is relatively fast in comparison to creep, only time-independent deformation mechanism of rock salt such as grain rearrangement, cataclasis (grains brittle failure because of intra-grain slips or local stress concentrations), and grain crystal plasticity have a chance to occur. The grain boundaries of the wet specimen, which are mainly composed of the added brine to the salt grains, facilitate the dislocation (rearrangement) of the grains during the compression and decrease cataclases compared to the dry specimen. This difference in the developed deformation mechanisms explains the higher reduction of the porosity of the wet specimen in comparison to the dry specimen.

By plotting ϕ of the specimens being compressed against the logarithm of the applied axial stresses, a point can be found on the curves where the relationship of $\log_{10}\sigma_1$ versus ϕ becomes linear (Fig. 4) and is denoted in this study as the critical porosity. This critical porosity value can be physically explained as the point where the dominant deformation mechanisms transition from grain rearrangement and cataclasis to grain crystal plasticity and eventually grain boundary diffusion. The critical porosities of the specimens being compressed in dry and wet manners were found to be 32% and 37%, respectively. As shown in Fig. 4, the wet specimens reached the critical porosity earlier compared to the dry specimens due to the effects of added brine to the grain boundaries. Eqs. (5) and (6) show the fitted lines to the 1D compression of the specimens during dry and wet 1D compressions after reaching the critical porosities, respectively.

$$\phi_L = -35.94\log_{10}\sigma_1 + 90.44 \quad \left(R^2 = 0.999\right) \tag{5}$$

$$\phi_L = -34.25\log_{10}\sigma_1 + 85.1 \quad \left(R^2 = 0.998\right) \tag{6}$$

Porosities of the specimens versus the applied axial stresses during unloading and reloading of the specimens for the dry and wet 1D compressions were fitted to Eqs. (7) and (8), respectively. The fitted lines representing the unloading-reloading curves started to diverge from the actual reloading curves as the axial stresses became closer to the axial stresses on the loading path. The lower values of R^2 for Eqs. (7) and (8) are caused by the deviation of the fitted lines from the actual reloading curves. During the reloading of the material when σ_1 advances towards the loading curve, the reapplied stresses on the specimen can cause further crystal plasticity and grain boundary diffusion, which decreases the porosity of the specimens at a higher rate.

$$\phi_R = -0.228\log_{10}\sigma_1 \quad \left(R^2 = 0.985\right) \tag{7}$$

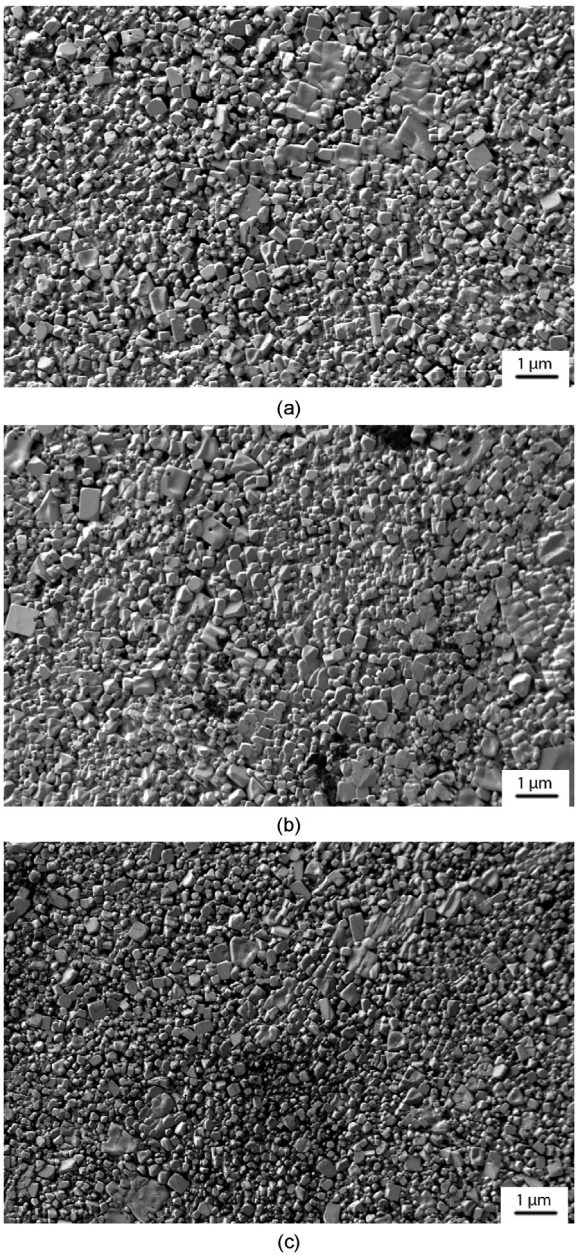

Fig. 5. SEM scan of a dry specimen: (a) Top layer; (b) Middle layer; and (c) Bottom layer.

$$\phi_R = -0.399\log_{10}\sigma_1 \quad \left(R^2 = 0.983\right) \tag{8}$$

The slope of the lines fitted to the unloading-reloading phases of dry and wet 1D compressions in both normal and semi-logarithmic scales are marginal and quite close to zero (Eqs. (3), (4), (7) and (8)). These nearly horizontal slopes show that the elastic deformations within the specimen are marginal and the compressed specimen nearly maintains its final porosity after unloading.

The averages of the porosities of dry and wet specimens at the end of 1D compression of each layer were 8.1% and 6.4%, respectively (Fig. 4). The 1-h compression after the 1D compression of the individual layers caused a decrease in the averages of the porosities of dry and wet specimens to 6.9% and 2.6%, respectively (Table 1).

This 1-h compression contributed to the activation of time-dependent deformation mechanisms within the specimens such as grain boundary diffusion and pressure solution. However, pressure solution can only occur in the presence of water at the grain boundaries. Pressure solution is the simultaneous development of grain dissolution at highly stressed grain boundaries, its diffusion into the wet grain boundary, and its precipitation at less stressed grain boundaries, which justifies the greater reduction in the porosities of the wet specimens. Lastly, the averages of the final porosities of dry-annealed and wet-annealed specimens were measured to be 1.6% and 0.8%, respectively (Table 1). Time-dependent deformation mechanisms continued to cause a decrease in the porosity of the specimens during the annealing process. Both dry and wet specimens exhibited a considerable decrease in ϕ after the annealing process. Annealing in polycrystalline rock salt recrystallizes the compressed grains (crystals), which further results in a reduction in the porosity of the material (Ding et al., 2016).

5. Scanning electron microscopy (SEM)

One representative specimen of each of dry, dry-annealed, and wet-annealed types were cut across their height into five disks with equal thicknesses of 8 mm. The bottom surface of the top disk corresponding to the middle of the top layer, the top surface of the middle disk corresponding to the middle of the middle layer, and the top surface of the bottom disk corresponding to the middle of the bottom layer were selected for further examination using SEM method. Each disk was sanded and further polished using P3000 sandpaper to achieve an average surface roughness of $R_a = 0.018$ μm. A relatively low electron high tension (EHT) voltage of 1 kV was employed to prevent the scanned surfaces from being charged because rock salt is not electrically conductive and the scanned specimens were not coated with a conductive layer. Type II secondary electron (SE2) signals were used by the SEM detector to scan the disks; thus, the scan would reflect a two-dimensional (2D) topography of the surfaces.

Figs. 5–7 show the 2D scans of representative dry, dry-annealed, and wet-annealed specimens where scans a, b, and c show the top, middle, and bottom of the cross-section of the specimens, respectively. Local porosity and average grain size of each scan were calculated using Avizo (FEI Visualization Sciences Group, 2018) image processing software. Black pixels of the scan were segmented using a threshold module to represent the voids inside the specimen. The local porosity of the scan was calculated by dividing the area of the voids by the total area of the scan. The grains of the specimen shown on the scans were found by labeling function of Avizo and the average grain size of the scan was determined by using label analyses function. Table 2 summarizes the values of porosities and average grain sizes of the scans. Across the height of the scanned dry specimen, the porosity and average grain size increased from the top to the bottom layers. The presence of sharp-cornered cubical grains shows the dominance of cataclases within the dry specimen. Moreover, grain boundary diffusion can also be noted between the grains. The 1-h compression in the process of preparing the specimen impacted the top layer more than the layers beneath it. The axial stresses applied to the specimen during the 1-h compression specifically intensified cataclases within the top layer of the specimen, which decreased the porosity of the top layer (Fig. 5).

The dry-annealed specimen also exhibited well-defined cubical grains, which indicated the dominance of cataclases; however, the grains had rounded corners (Fig. 6). Grain boundary diffusion and recrystallization of the grains can also be seen in the scans displayed in Fig. 6. It is worth mentioning due to the small grain size in the dry and dry-annealed specimens, crystal plasticity of the grains cannot be investigated. The average grain size within the dry-annealed specimen increased from the top layer to the bottom layer, which is the same pattern as the dry specimen. The similarity of the increase in the porosity of the specimen from the top layer to the bottom layer in dry and dry-annealed specimens is inherited from the 1-h compression step, where the two types of specimens were compressed using the same procedure. Moreover, the mentioned similarity shows that annealing increased the size of the grains proportional to their initial sizes.

Larger grains of the wet-annealed specimen, which were not perfectly cubical in shape, show that cataclasis was not the dominant deformation mechanism in the 1D compression of wet rock

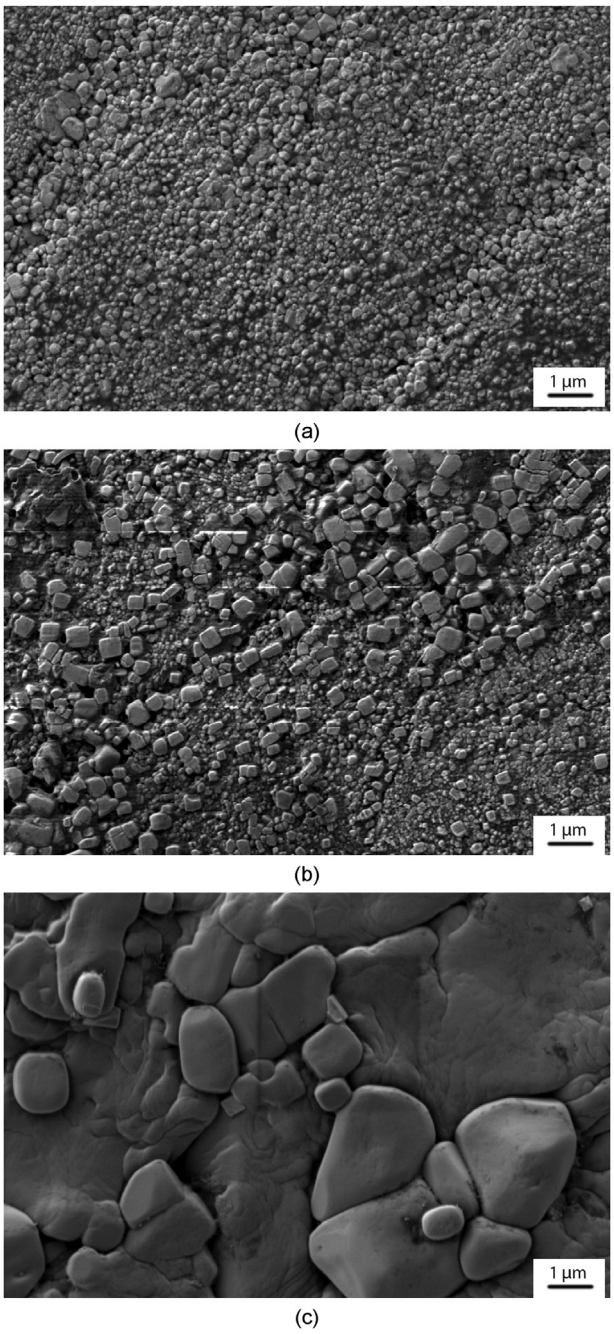

Fig. 6. SEM scan of a dry-annealed specimen: (a) Top layer; (b) Middle layer; and (c) Bottom layer.

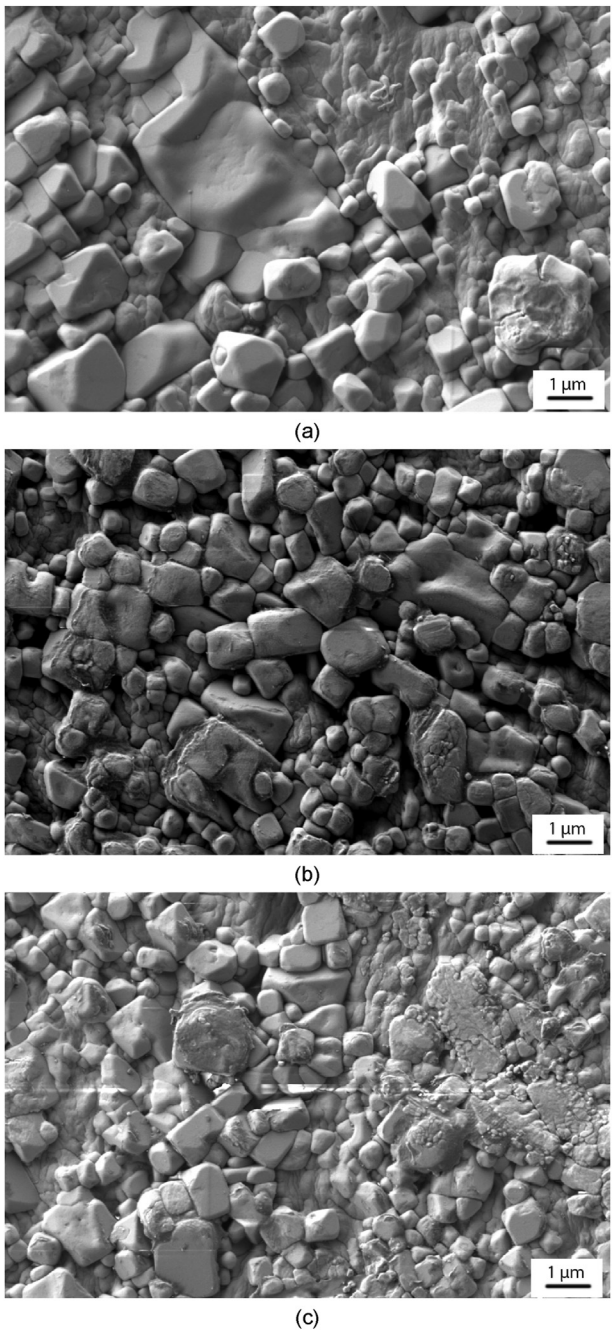

Fig. 7. SEM scan of a wet-annealed specimen: (a) Top layer; (b) Middle layer; and (c) Bottom layer.

Table 2
Porosity values and average grain sizes of different layers of representative dry, dry-annealed, and wet-annealed specimens.

Specimen	Layer	Porosity (%)	Average grain size (μm)
Dry	Top	5.8	0.13
	Middle	6.8	0.15
	Bottom	8.1	0.18
Dry-annealed	Top	1.9	0.17
	Middle	3.1	0.25
	Bottom	1.2	0.78
Wet-annealed	Top	0.8	0.67
	Middle	1.3	0.6
	Bottom	0.6	0.63

salt. Because of the larger grain size, the SEM scans of the wet-annealed specimen demonstrate the crystal plasticity imposed on the grains, where some grains have eventually fractured. Irregular diffused grain boundaries also point out to the pressure solution that has occurred inside the specimen during the 1-h compression of the specimen. Moreover, the recrystallization developed during the annealing process is clearer compared to the dry-annealed specimen. In contrast to the dry specimen, the dry-annealed and wet-annealed specimens possessed a lower porosity within the top and bottom layers compared to the middle layer (Figs. 6 and 7). From the macroscopic point of view, during the annealing of the material, the air and water inside the voids move out of the specimens. The purge of the fluid from the specimen depends on the distance from the void to the outside of the specimen and the interconnectivity of the voids throughout the specimen. Therefore, the voids enclosed inside the middle layer have a lower chance to exit the specimen.

A comparison amongst the variation of average grain sizes and porosities in the layers of different specimens shows that wet-annealed specimens exhibited a more uniform profile of average grain size and porosity with their height. Besides the global porosities in Table 1, the local porosities of the specimens obtained from Figs. 5–7 show that annealing of the specimens decreases the porosities of the specimens significantly.

6. Unconfined compression experiments

Two specimens of each type of prepared specimens were tested in unconfined compression experiments at 20 °C. The test equipment included a 44.5 kN (10,000 pounds) servo-automated load frame coupled with a 44.5 kN load cell and a 76.2 mm (3 in) range linear variable differential transformer (LVDT). The specimens were compressed at a constant strain rate of 1.7×10^{-4} s^{-1} according to ASTM D7012-14 (2014).

Fig. 8 shows the results of the unconfined compression experiments on dry specimens (D_1 and D_2), dry-annealed specimens (DA_1 and DA_2), wet specimens (W_1 and W_2), and wet-annealed specimens (WA_1 and WA_2). Table 3 summarizes the unconfined compressive strength (UCS or σ_u) and axial strain (ε_1) of the specimens at failure. Dry specimens showed an average σ_u of 64.3 MPa which was higher than σ_u of dry-annealed specimens (39.6 MPa). Bourcier et al. (2013) reported that polycrystalline rock salt specimens with smaller average grain size possess a higher σ_u. Smaller average grain size inhibits the formation of connected crystal dislocations. Moreover, dry specimens have high porosity grain boundaries compared to dry-annealed specimens, which are naturally immobile at room temperature (Guillope and Poirier, 1979). The immobility of grain boundaries resulted in an increase in σ_u of the material and reduced its ductility, explaining why dry specimens had lower ductility, $\varepsilon_1 = \sim 2.9\%$ at failure, compared to the other specimens.

Wet specimens had a σ_u of 16.1 MPa on average, which was the lowest compared to the other three types of specimens. The presence of water within the grain boundaries of salt crystals can cause weakening of the material. This weakening is associated with increased inter-granular deformation, grain boundary diffusion, and pressure solution in wet polycrystalline rock salt. Comparing σ_u of wet to dry specimens shows the effects of the weakening on σ_u of wet specimens. Moreover, wet specimens reached steady-state flow stress at $\varepsilon_1 = \sim 2\%$ and showed work-softening after approximately $\varepsilon_1 = 3.5\%$. The water within the grain boundaries of wet specimens also increased the ductility of the material due to enhanced inter-granular deformation, grain boundary diffusion, and pressure solution in the specimens.

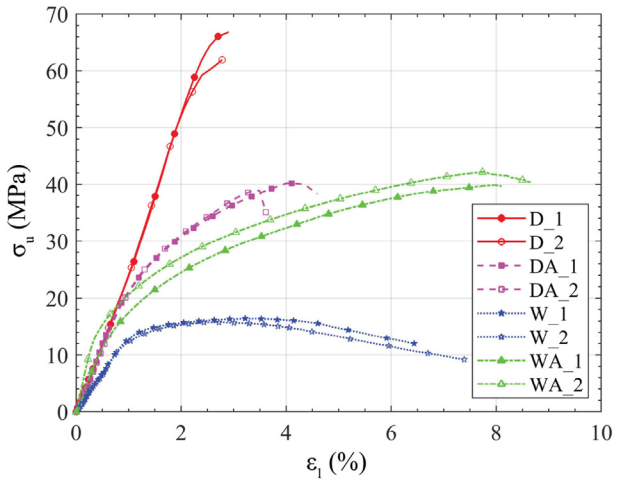

Fig. 8. Axial stress versus axial strain during unconfined compression experiments on two dry, dry-annealed, wet, and wet-annealed specimens.

Table 3
Unconfined compression experiment results of the polycrystalline rock salt specimens at room temperature.

Specimen	UCS, σ_u (MPa)	Axial strain at failure (%)
D_1 (dry)	66.8	2.9
D_2 (dry)	61.9	2.8
DA_1 (dry-annealed)	40.2	4
DA_2 (dry-annealed)	39	3.4
W_1 (wet)	16.4	6.4
W_2 (wet)	15.8	9.2
WA_1 (wet-annealed)	39.9	8
WA_2 (wet-annealed)	42.1	7.8

Wet-annealed specimens exhibited a completely different behavior in the unconfined compression experiment compared to wet specimens. Wet-annealed specimens did not show weakening. During the annealing process, wet-annealed specimens lost most of the water within the grain boundaries and the porosities of the specimens were decreased on average from 2.6% to 0.8%. The evaporation of the water around the grain boundaries decreased the inter-connectivity of wet grain boundaries, resulting in sparse wet grain boundaries within mostly dry grain boundaries. Moreover, annealing grew the size of the grains inside the polycrystalline media resulting in an increase in the grain to grain contacts and more interlocking inside the wet-annealed specimens. The changes in the properties of the grain boundaries, porosities, and grain sizes of the wet-annealed specimens after annealing led to work-hardening in the material during the unconfined compression experiments after about 0.8% axial strains. The σ_u value of wet-annealed specimens increased to 41 MPa as a result of the aforementioned changes within the specimen.

Comparing the results obtained from the unconfined compression experiments on wet compressed specimens to dry compressed specimens, the wet compressed specimens showed a more ductile behavior. This increase in ductility is a direct result of increased grain boundary mobilities due to the presence of water within grain boundaries of wet compressed specimens. Moreover, the bedding planes that were observed between the layers of the dry and dry-annealed specimens tend to obstruct crystal dislocations during the unconfined compression experiments which cause a more brittle response of the material.

7. Conclusions

The relationships between the porosity and the applied axial stresses in dry and wet 1D compressions of polycrystalline rock salt were fitted using decaying exponential models. The porosity in wet 1D compression decreased at a higher rate when compared to the dry ones due to the presence of water during the compression that facilitated the dislocation of the grains. When the porosity is plotted versus the logarithm of the applied axial stress, both dry and wet 1D compressions show a linear relationship between porosity and the logarithm of axial stress after reaching unique critical porosity values. The critical porosities of dry and wet 1D compressions were found to be 32% and 37%, respectively. The relationships of the porosity and the applied axial stress in dry and wet 1D compressions in unloading and reloading regions were fitted with linear trend lines that have slopes close to zero, suggesting that the elastic deformations during the 1D compression are marginal and nearly the entire deformation is non-recoverable.

Wet compressed specimens possessed a lower porosity after the 1-h compression when compared to dry compressed specimens because of the development of pressure solution deformation mechanism. Annealing of both the dry and wet specimens after the 1-h compression resulted in a decrease in their porosities and an increase in their average grain sizes. The local porosity of the non-annealed specimens increased from the top layer to the bottom layer, while the local porosities of the annealed were maximum in the middle layer. Wet-annealed specimens showed more homogeneity in local porosities and average grain sizes compared to the other types of the prepared specimens.

Dry specimens exhibited the highest UCS (64.3 MPa) compared to the other types of specimens. Moreover, dry specimens failed in a brittle manner. Dry-annealed specimens had a lower UCS of 39.6 MPa and exhibited a ductile behavior when compared to dry specimens. Wet specimens exhibited weakening during the unconfined compression experiments and their UCS was averaged at 16.2 MPa. Wet specimens had a ductile failure. Wet-annealed specimens had an increase in their average UCS to 41 MPa compared to wet specimens. Wet-annealed specimens had a ductile failure behavior.

The authors suggest studying the behavior of the prepared specimens in unconfined compression tests at elevated temperatures for future work. Moreover, conducting creep experiments on the prepared specimens can reveal valuable insights about their creep behavior. Conducting in-situ X-ray diffraction on granular rock salt under 1D compression can also help better understand the elastoplastic deformation of the individual grains, especially in fine-grained rock salt.

Declaration of competing interest

The authors declare that they have no known competing financial interests or personal relationships that could have appeared to influence the work reported in this paper.

Acknowledgments

This material is based on work supported by the National Science Foundation under Grant No. CMMI-1641054. Any opinions, findings, conclusions, and recommendations expressed in this material are those of the authors and do not necessarily reflect the views of the National Science Foundation. XRD and SEM were acquired at the Joint Institute for Advanced Materials (JIAM) Diffraction Facility of the University of Tennessee, Knoxville, USA. The

authors are grateful to Ibrahim Aklouk, Karen Abercrombie, Tyler Galyon, and Darcie Halliburton, undergraduate research assistants at the University of Tennessee, Knoxville, for their help in the preparation of the specimens. The authors also thank the anonymous reviewers who contributed constructive comments and suggestions to improve this paper.

List of symbols

ϕ	Porosity
σ_1	1D compression axial stress
R^2	Coefficient of determination
ϕ_L	Porosity on the loading path
ϕ_R	Porosity on the reloading path
R_a	Average surface roughness
σ_u	Unconfined compressive strength
ε_1	Axial strain

References

ASTM D7012-14, 2014. Standard Test Methods for Compressive Strength and Elastic Moduli of Intact Rock Core Specimens under Varying States of Stress and Temperatures. ASTM International, West Conshohocken, PA, USA.

ASTM D2216-19, 2019. Standard Test Methods for Laboratory Determination of Water (Moisture) Content of Soil and Rock by Mass. ASTM International, West Conshohocken, PA, USA.

Bourcier, M., Bornert, M., Dimanov, A., Héripré, E., Raphanel, J.L., 2013. Multiscale experimental investigation of crystal plasticity and grain boundary sliding in synthetic halite using digital image correlation. J. Geophys. Res. Solid Earth 118 (2), 511–526.

Ding, J., Chester, F.M., Chester, J.S., Zhu, C., Arson, C., 2016. Mechanical behavior and microstructure development in consolidation of nominally dry granular salt. In: Proceedings of the 50th US Rock Mechanics/Geomechanics Symposium. American Rock Mechanics Association (ARMA).

Ding, J., Chester, F.M., Chester, J.S., Zhu, C., Arson, C., 2017. Microcrack network development in salt-rock during cyclic loading at low confining pressure. In: Proceedings of the 51st US Rock Mechanics/Geomechanics Symposium. American Rock Mechanics Association (ARMA).

Dronkert, H., Remmelts, G., 1996. Influence of salt structures on reservoir rocks in Block L2, Dutch continental shelf. In: Geology of Gas and Oil under The Netherlands. Springer, pp. 159–166.

Dusseault, M.B., Rothenburg, L., Bachu, S., 2004. Sequestration of CO_2 in salt caverns. J. Can. Pet. Technol. 43 (11), 49–55.

Fam, M., Santamarina, J.C., Dusseault, M.B., 1998. Wave-based monitoring processes in granular salt. J. Environ. Eng. Geophys. 3 (1), 15–26.

FEI Visualization Sciences Group, 2018. Avizo. 9, 7 edition. FEI, Hillsboro, OR, USA.

Guillope, M., Poirier, J.P., 1979. Dynamic recrystallization during creep of single-crystalline halite: an experimental study. J. Geophys. Res. Solid Earth 84 (B10), 5557–5567.

Hansen, F.D., Leigh, C.D., 2011. Salt Disposal of Heat-Generating Nuclear Waste. Technical Report. Sandia National Laboratories, Albuquerque, NM, USA.

Ter Heege, J.H., De Bresser, J.H.P., Spiers, C.J., 2005. Dynamic recrystallization of wet synthetic polycrystalline halite: dependence of grain size distribution on flow stress, temperature and strain. Tectonophysics 396 (1–2), 35–57.

Holcomb, D.J., Zeuch, D.H., 1988. Consolidation of Crushed Rock Salt: Part I: Experimental Results for Dry Salt Analyzed Using a Hot-Pressing Model. Sandia National Laboratories, Albuquerque, NM, USA.

Hunsche, U., Hampel, A., 1999. Rock salt — the mechanical properties of the host rock material for a radioactive waste repository. Eng. Geol. 52 (3–4), 271–291.

Hwang, C.L., Wang, M.L., Miao, S., 1993. Proposed healing and consolidation mechanisms of rock salt revealed by ESEM. Microsc. Res. Tech. 25 (5–6), 456–464.

Knudsen, F.P., 1959. Dependence of mechanical strength of brittle polycrystalline specimens on porosity and grain size. J. Am. Ceram. Soc. 42 (8), 376–387.

De Las Cuevas, C., Pueyo, J.J., 1995. The influence of mineralogy and texture in the water content of rock salt formations. Its implication in radioactive waste disposal. Appl. Geochem. 10 (3), 317–327.

Lebensohn, R.A., Dawson, P.R., Kern, H.M., Wenk, H.-R., 2003. Heterogeneous deformation and texture development in halite polycrystals: comparison of different modeling approaches and experimental data. Tectonophysics 370 (1–4), 287–311.

Liang, W., Zhang, C., Gao, H., Yang, X., Xu, S., Zhao, Y., 2012. Experiments on mechanical properties of salt rocks under cyclic loading. J. Rock Mech. Geotech. Eng. 4 (1), 54–61.

Marques, F.O., Burg, J.-P., Armann, M., Martinho, E., 2013. Rheology of synthetic polycrystalline halite in torsion. Tectonophysics 583, 124–130.

Mills, M.M., Stormont, J.C., Bauer, S.J., 2018. Micromechanical processes in consolidated granular salt. Eng. Geol. 239, 206–213.

Mouritz, A.P., 2012. Strengthening of metal alloys. In: Mouritz, A.P. (Ed.), Introduction to Aerospace Materials. Woodhead Publishing, pp. 57–90.

Müller, C., Frühwirt, T., Haase, D., Schlegel, R., Konietzky, H., 2018. Modeling deformation and damage of rock salt using the discrete element method. Int. J. Rock Mech. Min. Sci. 103, 230–241.

Ostapenko, N.I., Sugakov, V.I., Shpak, M.T., 1993. Dislocations and optical properties of organic crystals. In: Spectroscopy of Defects in Organic Crystals. Springer, pp. 133–158.

Paneru, L.P., Bauer, S.J., Stormont, J.C., 2018. Thermal properties of consolidated granular salt as a backfill material. Rock Mech. Rock Eng. 51 (3), 911–923.

Peach, C.J., Spiers, C.J., Trimby, P.W., 2001. Effect of confining pressure on dilatation, recrystallization, and flow of rock salt at 150 °C. J. Geophys. Res. Solid Earth 106 (B7), 13315–13328.

Pouya, A., 1991. Correlation between mechanical behaviour and petrological properties of rock salt. In: Proceedings of the 32nd US Symposium on Rock Mechanics. USRMS.

Sannemann, D., 1968. Salt-stock families in northwestern Germany. In: Diapirism and Diapirs: a Symposium. American Association of Petroleum Geologists. https://doi.org/10.1306/M8361C16.

Shen, X., Arson, C., 2019. An isotropic self-consistent homogenization scheme for chemo-mechanical healing driven by pressure solution in halite. Int. J. Solid Struct. 161, 96–110.

Shen, X., Arson, C., Ding, J., Chester, F.M., Chester, J.S., 2020. Mechanisms of anisotropy in salt rock upon microcrack propagation. Rock Mech. Rock Eng. 53 (7), 3185–3205.

Stormont, J.C., Lampe, B.L., Lynn, T.D., Bauer, S.J., 2017. Gas permeability of granular salt during consolidation. In: Proceedings of the 51st US Rock Mechanics/Geomechanics Symposium. American Rock Mechanics Association (ARMA).

Titler, R.V., Curry, P., 2011. Chemical Analysis of Major Constituents and Trace Contaminants of Rock Salt. Pennsylvania Department of Environmental Protection. Technical Report.

Trusheim, F., 1960. Mechanism of salt migration in northern Germany. AAPG Bull. 44 (9), 1519–1540.

Urai, J.L., Spiers, C.J., Zwart, H.J., Lister, G.S., 1986. Weakening of rock salt by water during long-term creep. Nature 324 (6097), 554–557.

Amirsalar Moslehy is a graduate teaching associate and research assistant at the University of Tennessee, Knoxville, USA. He obtained his BSc degree in Civil Engineering from Iran University of Science and Technology, Tehran, Iran in 2015, and his MSc degree in Geotechnical Engineering from University of Tehran, Tehran, Iran in 2017. He also obtained an MSc degree in Civil Engineering from University of Tennessee, Knoxville, TN, USA in 2020, while pursuing his PhD in Civil Engineering with a minor in Computational Science. His research interests include (1) experimental studies on the mechanical behavior of rock salt; (2) experimental studies on the constitutive behavior of granular material; and (3) numerical modeling of granular soil.